



Research Article

Green synthesized amino-PEGylated silver decorated graphene nanoplatform as a tumor-targeted controlled drug delivery system

Prakash Kumar Palai¹ · Aparna Mondal¹ · Chandra Kanti Chakraborti² · Indranil Banerjee³ · Kunal Pal³

© Springer Nature Switzerland AG 2019

Abstract

In this study design, the PEGylated silver decorated graphene nanocomposites (NGO-AgNPs-PEG) were successfully prepared by eco-friendly non-toxic green synthesis following a novel syn-graphenization method using the aqueous leaf extract of *Azadirachta indica* (*A. indica*) (neem) as reducing agent. The prepared Smart pH stimuli responded nanoplatform was thoroughly characterized by various analytical techniques. Since a functional nanocarrier is very essential for cancer therapy, it could quickly guide the loaded anticancer drug to the tumor site to decrease the side effect. In order to overcome the side effects of doxorubicin (DOX), an anticancer drug, it was incorporated into amino PEGylated NGO-AgNPs nanocomposites. Considering drug loading and release studies, it may be concluded that improved drug loading efficiency (218%) and more pH-responsive controlled release (following Korsmeyer–Peppas model release kinetics) of DOX from NGO-AgNPs-PEG lead to a promising nanocarrier for the anticancer drug. The cytotoxicity study results, on HaCaT cell lines, indicated DOX-loaded PEGylated functionalized nanographene oxides, as compared to free DOX, had lesser harmful effect on normal cells than cancer cells. Increased cytotoxicity was exhibited in the cancerous cells (HeLa cell lines) treated with DOX loaded PEGylated silver functionalized nanographene oxide compared to covalently conjugated NGO-DOX. So, the effective delivery and release of the anticancer drug into acidic microenvironment of the targeted tumour cells would bring out higher therapeutic efficacy than pure NGO. Such a gold standard biocompatible PEGylated silver decorated NGO theranostic nanoplatform may be an excellent nano cargo for targeted and controlled drug delivery in cancer therapy.

Keywords Graphene oxide · Silver nanoparticles · Doxorubicin · Cytotoxicity · Tumor · Targeted drug delivery

1 Introduction

Considering the importance of chemotherapy in the treatment of different types of cancers, targeted drug delivery systems have been developed to specifically deliver chemotherapeutic agents at the cancer sites, bypassing side effects on normal cells [1]. As we know, the leaky

hypervascularized cancerous tissues have enhanced permeability and retention (EPR) effect for nanoscopic particles. The EPR effect is the basic mechanism behind passive targeting of controlled drug delivery in treatment of cancer [2].

Knowing the above mentioned information, nanoparticles might be considered as an important weapon to treat

Electronic supplementary material The online version of this article (<https://doi.org/10.1007/s42452-019-0287-9>) contains supplementary material, which is available to authorized users.

✉ Prakash Kumar Palai, prakash75s@yahoo.in; Aparna Mondal, aparnamondal@nitrkl.ac.in; Chandra Kanti Chakraborti, chandrakanti_12@rediffmail.com; Indranil Banerjee, indraniliiit@gmail.com; Kunal Pal, palk@nitrkl.ac.in | ¹Department of Chemistry, National Institute of Technology, Rourkela, Odisha 769008, India. ²Department of Pharmaceutical Technology, NSHM Knowledge Campus, Kolkata - Group of Institutions, 124, B.L.Saha Road, Kolkata, West Bengal 700053, India. ³Department of Biotechnology and Medical Engineering, National Institute of Technology, Rourkela, Odisha 769008, India.



SN Applied Sciences (2019) 1:269 | <https://doi.org/10.1007/s42452-019-0287-9>

Received: 28 January 2019 / Accepted: 19 February 2019 / Published online: 27 February 2019

cancer effectively. Environmentally safe method for silver nanoparticle synthesis is a vital area of research in nanomedicine due to eco-friendliness [3–5]. Green synthesis is a non-toxic method due to very less or non-consumption of hazardous materials on the surface of nanomaterials. Biosynthesized nanoparticles by green synthesis are normally biocompatible and have more biomedical applications [6, 7]. Furthermore, the phytochemical constituents of *Azadirachta indica* (*A. indica*) (neem) can block cancer growth, and they have strong reducing properties [8–10].

The reinforcement of graphene and its derivatives has produced unique outcomes in controlled and targeted drug delivery. High strength light weight structural graphene nanocomposites can be synthesized for biomedical application. Recently, metal nanoparticles are enormously used as theranostic agent for treatment of cancer [7]. Different functional groups and lattice defects of graphene favor the nucleation, size control and entrapment of metal nanoparticles [11, 12]. Among different types of method for synthesis of metal decorated graphene nanocomposites, syn-graphenization has major advantage of direct contact between graphene sheets and metal nanoparticles followed by homogeneous distribution and stabilization of nanoparticles on 2D graphene sheet [13, 14].

Due to removal of functional groups from graphene sheets during reduction process, the reduced graphene oxide (RGO) has greater tendency of agglomeration unless stabilized with the help of polymers by surface functionalization [15, 16]. Main mechanisms for interaction between the surfaces of graphene oxide and target molecules are mainly non-covalent functionalization and covalent functionalization [17].

Amino PEGylation of graphene oxide involves activation of carboxylic acid groups on graphene oxide by 1-ethyl-3-(3-dimethylaminopropyl)-carbodiimide (EDC) [18, 19]. Furthermore, PEGylated graphene oxide has greater dispersability in organic solvents than pure GO [1].

PEG is an excellent polymer for biomedical applications. The conformational cloud by PEG over the charged carrier reduces opsonisation and uptake by the reticuloendothelial system (RES) [20]. The development of an effective sterically hindering cloud on the surface of nanocomposites is mainly dependent on the molecular weight of PEG and mechanism of attachment of PEG to the surface of nanomaterials [7, 21].

As we know that PEG with a molecular weight below 400 Da undergoes degradation by alcohol and aldehyde dehydrogenases which are toxic to body, but the molecular weight below 20 kDa is suitable for urinary excretion, on the other hand, greater molecular weight of PEG (greater than 40–60 kDa) is unsuitable for urinary excretion, and hepatic clearance is the principal mechanism of its excretion [12, 22]. To bypass these uncertainties, multi

arm PEGs, like amino PEG, have been used that form low molecular mass PEGs which can be cleared more readily after metabolism in the body [12, 19]. It is already reported that during biosynthesis and PEGylation, the graphene oxide is partially reduced. The sp^2 grid on GO involves covalent functionalization with PEG and loading of aromatic compounds like Doxorubicin (DOX) imparts π - π interactions between aromatic rings and reduced graphene oxide nanosheets, providing stability for both the components [1, 7].

As an anthracycline antibiotic, DOX has been extensively used for treatment of cancer [7]. However, DOX has intense side effects such as hair loss, vomiting, tissue inflammation and cardiac muscle injury due to accumulation in different organs during systemic circulation. The idea of nanocarrier targeted controlled drug delivery could quickly guide the loaded drug to the tumor site to decrease the side effect to normal cells [23]. Hence, for targeted controlled delivery of DOX, a functionalized nanocarrier with magnificent drug loading capacity is very essential for treatment of cancer. DOX with carbonyl groups and amino group could interact with NGO surface via π - π interactions [24]. This π - π interaction is attributed to a non-covalent type of functionalization that imparts targeted controlled release of drug [25]. Furthermore, the designed and developed DOX loaded PEGylated NGO-AgNPs drug delivery systems may show remarkable retardation of cancer cell proliferation than pure NGO and AgNPs loaded with the drug.

An added benefit of graphene for anticancer drug delivery is its pH-guided drug delivery behavior, where increased drug release at acidic pH (pH 5.0–5.6) provides efficient intracellular drug release in acidic microenvironment of cancer cells [26, 27]. Smart pH stimuli responded PEGylated graphene nanocomposites are anticipated for avoiding RES uptake and prolongation of nanocarrier systemic circulation [28]. PEGylated silver decorated graphene nanocomposites may be an efficient drug cargo by protecting the loaded drugs from enzymatic degradation, increasing drug loading, improving drug bioavailability, and assisting controlled targeted drug release. “Smart” PEGylated NGO-AgNPs can be used to bring about targeted controlled drug release by interaction with functional groups at the pore entrance. As a result, the drug loaded in pore cannot be released freely unless there would be change in pH [2, 12, 28].

In this article, the PEGylated silver decorated graphene nanocomposites were successfully prepared by green synthesis following syn-graphenization method. The green chemistry approach for the design of PEGylated silver decorated graphene nanocomposites utilizing ‘*Azadirachta indica* (*A. indica*) (neem)’ leaf extract where the neem extract acted as both reducing agent and stabilizing agent.

Aforementioned approach was adopted because there is no previous report on green synthesis of theranostic platform utilizing amino PEG tethered NGO-AgNPs nanocomposites for in vivo drug delivery application to treat cancer. Considering the benefits (mentioned earlier), nanocomposites were prepared by incorporating amino PEG (molar mass 5000 Da). Moreover, PEGylated NGO-AgNPs nanocomposites were also produced using doxorubicin (DOX) as a model antitumor drug. Finally, characterisation, drug release, and cytotoxicity studies of the prepared drug loaded smart nanocomposites were carried out.

2 Materials and methods

2.1 Materials and reagents

Experiments were carried out using Ultrapure Millipore water. Graphite powder (99.5%) was purchased from HiMedia Laboratories, Mumbai, India; Sulfuric acid from Finar Reagents, Ahmedabad, India; Hydrochloric acid from Merck Specialities Pvt. Ltd., Mumbai; potassium permanganate from Finar Reagents, Ahmedabad, India; and Hydrogen peroxide from SDFCL Limited, Mumbai. Silver nitrate (AgNO_3 ; 99.0%), Amine functionalized methoxy-polyethylene glycol (mPEG-NH₂; Mw 5000), 1-ethyl-3-(3-dimethylaminopropyl) carbodiimide hydrochloride (EDC; 99.0%) 3-(4, 5-dimethylthiazol-2-yl)-2,5-diphenyl-tetrazolium bromide (MTT), N-hydroxy succinimide (NHS; 99%) and N-acetylcysteine (NAC; $\geq 98\%$) were obtained from Sigma-Aldrich (USA). Doxorubicin hydrochloride (DOX; 98.0–102.0%) was procured from Cayman chemical company (USA). All chemicals were used as received.

2.2 Nanoformulation preparation method

2.2.1 Ecofriendly synthesis of NGO

Commonly graphite is oxidized by treatment with KClO_3 , KMnO_4 and fuming NaNO_3 in presence of concentrated H_2SO_4 . Oxidation of graphite to graphine oxide by using the above mentioned agents involves the generation of the toxic and explosive gas(es) like NO_2 , N_2O_4 , and/or ClO_2 . For the preparation of GO, like Lei et al. [29] modified Hummers method was further modified in the present investigation to get rid of toxic gases and some impurities. This was done by using KMnO_4 in presence of concentrated H_2SO_4 along with drop wise addition of dilute aqueous solution of H_2O_2 . Furthermore, the above ecofriendly synthesized aqueous suspension of GO was stirred up to 12 h and ultrasonicated for 30 min to get exfoliated GO. Subsequently, the prepared NGO was filtered and freeze dried to carry out different characterisation studies.

2.2.2 Preparation of aqueous leaf extract of *A. indica*

Finely chopped 40 g of washed, dried leaves of '*Azadirachta indica* (*A. indica*) (neem)' were mixed with 200 ml of Millipore water in a 300 ml Erlenmeyer flask and steam distilled at 100 °C for 15 min with continuous stirring in order to obtain light green colour aqueous suspension. Then the cooled filtered extract was centrifuged at 7000 rpm for 15 min to separate the solid content. The extract of neem leaves was stored in an air tight container at 4 °C for its (further) use in synthesis of nanoparticles.

2.2.3 Green synthesis of silver decorated NGO nanocomposites

Reducing silver nitrate (AgNO_3) with aqueous extract of neem leaves in aqueous NGO solution, silver decorated NGO nanocomposites were synthesized. Forty milliliter of 10^{-3} (M) of AgNO_3 solution were mixed with colloidal dispersion of NGO (1 mg/ml), which was prepared by using deionized water following ultra-sonication for 1 h. This mixture was transferred to a volumetric flask after sonication for another 30 min. Aqueous leaf extract of neem (like 6, 8 and 10% v/v) was added separately to each of NGO and AgNO_3 mixture drop wise under vigorous stirring at room temperature for 1 h. This procedure was repeated thrice for optimization of reducing agent by changing the volume of aqueous leaf extract of neem by 6, 8 and 10% v/v to ensure optimum synthesis of AgNPs on NGO nanopatform. The color of the mixtures gradually changed to dark-brown, resulting in synthesis of nanocomposite. The AgNPs were formed by the ecofriendly reduction of Ag^+ ions utilizing the herbal reducing agent. The presence of AgNPs was primarily validated by appearance of plasmon absorption band in UV-Vis spectra. After proper ultra-centrifugation and washing by deionized water, the NGO-AgNPs composites were dried by lyophilization.

2.2.4 Preparation of functionalised PEGylated silver decorated graphene nanocomposites (NGO-AgNPs-PEG)

In order to bypass the toxicity profiles of the graphene-based nanomaterials, different biocompatible polymers like chitosan [29], dextran [30], and polyethylene glycol [18] were used as functionalizing agents to enhance biocompatibility of functionalized graphene. The hydrophilicity, colloidal stability and biocompatibility of the NGO-AgNPs nanocomposites may be improved by amino PEGylation. For amino PEGylation, 10 ml of mPEG-NH₂ (50 mg/ml) was mixed with 18 ml of metallic NGO nanocomposite (0.5 mg/ml), and the mixture was ultrasonicated for 1 h. The oxygen containing functional groups

were activated by incorporating 6 ml of EDC (20 mg/ml) and 6 ml of NHS (16 mg/ml) to the NGO amino PEG dispersion with vigorous stirring for 12 h, and then functionalized NGO-AgNPs-PEG nanocomposite was washed and purified by using Millipore water. Hydrophilic biocompatible PEGylated graphene nanocomposite thus obtained was used for loading of DOX.

2.2.5 Preparation of drug encapsulated PEGylated graphene silver nanocomposites

DOX loading was carried out by the addition of different amounts of drug with the pure graphene oxide and PEGylated graphene silver nanocomposite. The nanocomposites were added to each of the aqueous solutions of drug (containing 50 µg/ml) to produce formulations like F_0 (10 µg/ml of GO), F_1 (1 µg/ml of NGO-AgNPs-PEG), F_2 (10 µg/ml of NGO-AgNPs-PEG), and F_3 (100 µg/ml of NGO-AgNPs-PEG) and were kept in shaking incubator at 28 °C for 24 h for optimum drug loading. After 24 h, dialysis was carried out for removal of unloaded DOX, and its progress (by dialysis) was monitored by UV-Vis spectroscopic analysis. Then the purified drug loaded nanocomposites were lyophilized to obtain DOX-loaded NGO-AgNPs-PEG nanocomposites for further qualitative analysis.

2.3 Characterization techniques

UV/Vis spectra of pure NGO, pure DOX, NGO-AgNPs, and NGO-AgNPs-PEG-DOX dispersions were recorded with a Shimadzu 160 spectrophotometer within 200–800 nm wavelengths [31]. Initially, the λ_{\max} of DOX was determined. The absorbance of pure DOX solutions containing 2, 4, 6, 8, 10, 20 and 50 µg/ml at its λ_{\max} was determined. For the determination of concentration of DOX in an unknown sample, the standard curve or calibration curve was plotted by taking its respective values of concentration vs absorbance.

Fourier transform infrared spectroscopy-attenuated total reflectance (FTIR-ATR) analysis was carried out by using a Perkin Elmer Spectrum RX. In order to determine purity and chemical compatibility, pure NGO, mPEG-NH₂, AgNPs, NGO-AgNPs-PEG, DOX, and NGO-AgNPs-PEG-DOX were mixed separately with spectroscopic grade potassium bromide (KBr) powder and then after compression sample loaded KBr pellets were scanned in the range of 400–4000 cm⁻¹ [31].

By keeping the gold coated samples on aluminum stub using Nova Nano FESEM 450 with an accelerating voltage of 20 kV, Field emission scanning electron microscopic (FESEM) analysis was done to study surface morphology of NGO, AgNPs and NGO-AgNPs, AgNPs present in the nanocomposites. Elemental analysis of NGO-AgNPs was

done using energy dispersive spectroscopy by Nova Nano FESEM/EDS 450, applying 15 kV accelerating voltages [31].

Microstructural investigation of the selected area of NGO, AgNPs and NGO-AgNPs was carried out on a copper grid using high-resolution transmission electron microscopy (HRTEM, JOEL-JEM 2100) with an accelerating voltage of 200 kV at around 28 °C. The selected area electron diffraction (SAED) measurement of pure NGO, pure AgNPs and AgNPs in NGO-AgNPs nanocomposite was performed [32].

To determine change in crystallinity after incorporation of AgNPs into NGO, XRD studies of pure NGO and NGO-AgNPs nanocomposite were performed at 2θ values from 5° to 80° using the Bruker D8 ADVANCED diffractometer equipped with the CuKα line at 1.5418 Å as radiation source [31].

The zeta potential values of NGO, NGO-AgNPs-PEG, pure DOX and NGO-AgNPs-PEG-DOX were determined by a Malvern Zetasizer (Malvern Instruments, UK) to ascertain stability of nanocomposites in biological fluid. The zeta potential distribution values were obtained from the graph between zeta potential and total counts [7].

From the above-mentioned characterization techniques, it is clear that identical samples were not used for different tests. Considering the requirements, only appropriate samples were included.

2.4 In vitro studies

2.4.1 Drug entrapment efficiency (%EE) and drug loading content (%DLC)

DOX content in NGO-DOX and NGO-AgNPs-PEG-DOX nanocomposite was determined by dissolving the DOX-loaded nanocomposites in dimethylformamide (DMF). The concentration of DOX in the DMF was measured from the UV-Vis spectra at 480 nm. The amount of DOX, which was incorporated into the PEGylated graphene nanocomposites, was calculated by deducting the amount of supernatant with free DOX from the total amount of DOX that had been initially added. Drug entrapment efficiency and drug loading content of NGO-DOX and NGO-AgNPs-PEG-DOX nanocomposites were calculated according to the formula followed by Li et al. [33].

2.4.2 Drug release response

The release behavior of DOX from DOX-loaded graphene oxide and functionalized PEGylated graphene nanocomposites was also evaluated by dialysis. One milliliter each of DOX-loaded NGO (50 mg/ml) and functionalised PEGylated graphene silver nanocomposites solutions (50 mg/ml) were sealed separately in molecular weight

cut-off (MWCO: 3500 Da) membrane and were dialyzed against 20 ml of phosphate buffered saline at pH of either 7.4 or 5.4 at 37 °C on horizontal shaker. At different time points, aliquot of the released solution (PBS) with DOX was taken out and periodically replaced with fresh PBS (volume equivalent to the volume of fraction withdrawn) to maintain a constant volume. Amount of released DOX from DOX-loaded GO and functionalised PEGylated graphene silver nanocomposites was obtained at 0.5, 1, 2, 3, 4, 5, 6, 7, 8, 12, 24, 36, 48, 72, 120 h by measuring concentrations of released DOX in solution outside of MWCO membrane by UV–Vis spectroscopic analysis at a λ_{\max} of 480 nm [34]. To improve the quality of analytical data and accuracy, the aliquots were collected at three different points of dialysis solution and average of percentages of drug release was considered.

2.4.3 Release kinetics

In order to understand the kinetic and mechanism of DOX release, results of the in vitro drug release study of the nanoformulations were fitted with different kinetic models like zero order release kinetics, first order release kinetics, Higuchi's model, and Korsmeyer–Peppas model [35]. The release exponent of Korsmeyer–Peppas model (n value) could be used to characterize pattern of DOX release from different nanocomposites. In order to compare the release data of the formulations, dissimilarity (f_1) and similarity (f_2) factors were considered.

2.5 Cytotoxicity study

The cytotoxicity of different samples was ascertained against a cancer cell line, HeLa cell line (cervical cancer of a young African-American woman, Henrietta Lacks), and another normal cell lines, HaCaT (human keratinocyte cell line), using MTT assay [36]. The cells cultured in DMEM (Dulbecco's Minimum Essential Medium) were seeded at a density of 2×10^4 cells/ml in a 96 well plate containing 100 μ l of the respective culture medium in each well and allowed for 24 h proliferation. NGO, neem leaf extract, AgNPs, NGO-AgNPs, NGO-AgNPs-PEG, pure DOX, NGO-DOX, and NGO-AgNPs-PEG-DOX at various concentrations were separately added to the cells and incubated for 48 h. MTT (10 μ l of 5 mg/ml stock) was added 6 h before the end point and their cell viability was evaluated by MTT assay after 48 h. Aliquot of medium was withdrawn, and dimethyl sulfoxide (100 μ l) was added for dissolving the formazan byproduct. Percentage cell viability was calculated by measuring absorbances (at 570 nm) of test sample and control by using a microplate reader.

The detail map of the surface features of the cell lines after treatment and nanocomposites embedded in the

cells were captured by phase contrast microscopy in tapping mode.

3 Results and discussion

3.1 Characterization of graphene nanocomposites and drug

One main UV absorbance peak at 231 nm has been assigned to sp² hybrid regions of C–C and C=C bonds, and sp³ hybrid regions of the C=O bond denoted by a shoulder peak at about 303 nm (Fig. 1a). The overall features of UV spectrum and absorption peaks of synthesized GO are identical to that of the GO samples as reported in literature [37].

The values of λ_{\max} of DOX were found to be 234, 252, 288 and 480 nm which matches with the product information of Doxorubicin (Hydrochloride) supplied by Cayman chemicals (Fig. 1a). This result indicates the drug was pure, stable and free from impurities. The regression equation of standard curve was obtained as follows: $y = 0.015x + 0.008$, where y is the absorbance value and x is the concentration of DOX (Fig. 1b) (Table. S1). The R square value of the regression equation obtained from standard plot of DOX was found to be 0.999, indicating good linearity of UV–Vis measurement within DOX concentration in the range of 2–50 μ g/ml. Moreover, the standard deviations of the samples were all less than 0.1%, suggesting good precision of this method.

In the present study, like several investigations, the appearance of a characteristic sharp surface plasmon resonance band at $\lambda = 430$ nm (between 400 and 500 nm) implies the formation of AgNPs [38]. The reduction in progress of NGO was observed by UV–Vis spectroscopy. As shown in Fig. 1c, the intensity of two UV–Vis absorption peaks centred at 231 nm is due to presence of NGO. After reduction by neem extract, the peak at 231 nm gradually red-shifted to 269 nm, which may be attributed to electronic conjugation reaction [39]. The presence of Ag nanoparticles in the nanocomposite was confirmed by the UV–Vis spectra by appearance of surface plasmon resonance band at $\lambda = 436$ nm in the absorption spectrum of NGO-AgNPs nanocomposite (Fig. 1c) [40].

The sharp localized surface plasmon resonance (LSPR) peak between 400 and 500 nm did not shift to longer wavelengths with increasing the silver concentration both in AgNPs and NGO-AgNPs [32]. It indicates that addition of neem extract as a reducing agent prevents agglomeration of the nanocomposites. However, a 9 nm red shift accompanied with a narrowing of the plasmon resonance of AgNPs in NGO-AgNPs was observed after

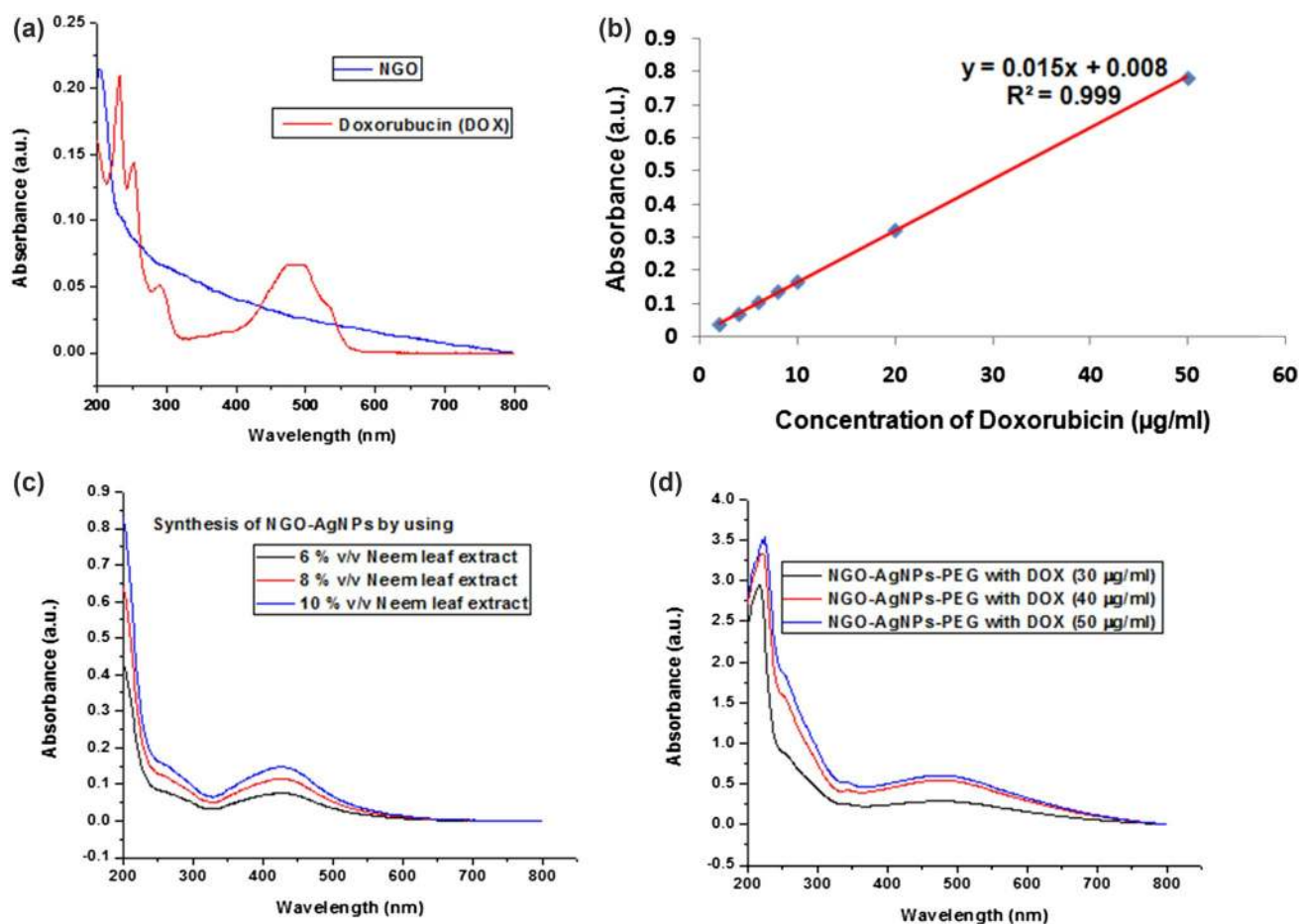


Fig. 1 **a** UV-Vis spectra of pure NGO and pure doxorubicin (DOX) in doubled distilled water. **b** Calibration curve of pure DOX solution. **c** UV-Vis spectra of synthesized NGO-AgNPs at different concentra-

tions of aqueous neem leaf extract. **d** UV-Vis spectra of DOX loaded NGO-AgNPs-PEG at different concentrations of DOX

reduction, which is most probably due to adsorption of AgNPs on NGO sheet which leads to change in size of AgNPs [41].

Absorbance of graphene silver nanocomposites synthesized at 1 h with various concentrations of neem extract was monitored by UV-Vis spectroscopy. The formation of stable AgNPs was confirmed by the appearance of LSPR band of AgNPs for these sample at around $\lambda_{\max} \sim 400\text{--}500$ nm in UV-Vis spectral pattern of NGO-AgNPs.

Moreover, the intensity of absorbance of AgNPs after 1 h is directly proportional to the concentration of neem extract (2–10% v/v). The maximum absorbance of AgNPs at 1 h was obtained by the reaction of 10% v/v of neem extract. The UV-visible spectroscopy was used to study the concentration dependent synthesis of AgNPs using 2–10% v/v of neem extract. The optimal reaction time has been found to be 1 h for reduction of AgNO_3 , as there is no further change in absorbance of the nanocomposites observed in UV-Vis spectrum (Fig. 1c).

After DOX loading to NGO-AgNPs-PEG at different concentrations, it was found that very minute shift in λ_{\max} value and plasmon bandwidth ($\Delta\lambda$) (10 nm), indicating higher in vitro stability of NGO-AgNPs-PEG nanocomposite (Fig. 1d). By comparing the UV-Vis spectra of pure DOX with DOX loaded nanocomposite, the values of λ_{\max} of DOX (234, 252, 288 and 480 nm) were found to be little bit changed in the nanocomposites. The peak at 234 nm remained unchanged indicating the presence of DOX. While the peak at 252 nm shifted to 269 nm, the peak at 288 nm was not prominent. Finally, the band at 480 nm merged with the LSPR band of AgNPs. This result indicates that there was a covalent interaction between NGO-AgNPs-PEG with DOX.

The FTIR spectra of GO sheet showed prominent adsorption bands for the carboxyl $\text{C}=\text{O}$ (1726 cm^{-1}), aromatic $\text{C}=\text{C}$ (1625 cm^{-1}), epoxy $\text{C}-\text{O}$ (1227 cm^{-1}), alkoxy $\text{C}-\text{O}$ (1094 cm^{-1}), and hydroxy $-\text{OH}$ (3407 cm^{-1}) groups [42]. The peak at 833 cm^{-1} represents the bending vibration of $\text{C}-\text{H}$ group. The oxidation of graphite powder to GO has

been confirmed by the presence of oxygen-containing functional groups [43]. The absorptive property of GO, was shown by a broad peak at 3407 cm^{-1} , is contributed by O–H stretch of H_2O molecules absorbed on its surface (Fig. 2) [44]. The results of UV–Vis and FTIR analyses demonstrate the successful synthesis of GO.

Figure 2 shows FTIR spectra of AgNPs which ascertain the purity and nature of the silver nanoparticles. A broad band observed at 3434 cm^{-1} was assigned to stretching vibrational mode of hydroxyl groups of absorbed water on AgNPs.

Moreover, sharp and strong absorption band at 1636 cm^{-1} was attributed to the stretching vibration of carbonyl (C=O) group of amide. The band at 1384 cm^{-1} was due to C–C and C–N stretching. The present study sample shows the characteristic band at 668 cm^{-1} (below 1000 cm^{-1}), which is ascribed to lattice vibration of silver oxide indicating the successful synthesis of silver nanoparticle [45, 46].

FTIR spectra of NGO-AgNPs nanocomposites were measured to confirm the successful formation of nanocomposites (Fig. 2). The most remarkable absorption band corresponds to the –OH stretching vibration, centred at 3550 cm^{-1} , is for the NGO-AgNPs nanocomposites; which is due to abundant amounts of hydroxyl groups on NGO. The shift of –OH stretching vibration to longer wave numbers in the nanocomposite is attributed to interactions between AgNPs and NGO [46]. The peaks at 1726 cm^{-1} for NGO and 1710 cm^{-1} in case of NGO-AgNPs nanocomposites can be assigned to the stretching vibration of carboxylic (C=O) groups [46, 47]. The residual sp^2 structure of NGO was confirmed with the C=C bending vibration at 1586 cm^{-1} . By comparing the spectra of pure Ag, the band patterns at 1384 cm^{-1} and 648 cm^{-1} (below 1000 cm^{-1})

indicate the presence of AgNPs in the nanocomposites. The peak at 809 cm^{-1} in NGO shifted to 833 cm^{-1} in NGO-AgNPs, which represents the bending vibration of C–H group [47].

However, the decrease in the intensity of the absorption bands of the oxygenated functional groups could be attributed to both the slight reduction of GO in the production process of NGO-AgNPs nanocomposite and the existence of the AgNPs on the surface of NGO nanosheets. The change and appearance of new peaks in the case of NGO-AgNPs nanocomposites revealed the interaction between silver ions of AgNPs and the un-reduced hydroxyl and carboxyl groups on the surface of the NGO with successful decoration of AgNPs on NGO [41, 48].

In FTIR spectra of mPEG-NH₂, the NH stretching mode was found between 3500 and 3450 cm^{-1} and the band observed at 1557 cm^{-1} corresponds to NH bending vibration of amino group. In addition, the peak at 2888 cm^{-1} was assigned to C–H stretching of methoxy ($\text{CH}_3\text{--O}$) groups.

The covalent bonding of mPEG-NH₂ and NGO-AgNPs was evaluated by FTIR spectroscopy. The carboxyl C=O band at 1726 cm^{-1} was significantly diminished after interaction of NGO with mPEG-NH₂. Simultaneously, new peaks for amide-I vibration modes of mPEG-NH₂ at 1638 and 1500 cm^{-1} were found on the FTIR spectra of NGO-AgNPs-PEG. These results indicate covalent binding and formation of ester linkage between mPEG-NH₂ and NGO-AgNPs. As an environmental friendly reducing agent, aqueous leaf extract of neem has been utilized for the chemical reduction. The excess aqueous leaf extract of neem was removed by repeated washing from NGO-AgNPs conjugate. However, incorporation of certain nitrogenous moieties into graphene nanosheets could not be blocked [49].

For FTIR spectra of pure DOX, the peaks for NH stretching and bending vibrations of amino group were observed at 3436 cm^{-1} and 1480 cm^{-1} , respectively. The band at 1628 cm^{-1} suggests the quinone group of DOX. In addition, the peak at 2885 cm^{-1} attributed to C–H stretching may be due to the methoxy group ($\text{CH}_3\text{--O}$) [36].

After DOX was incorporated onto NGO-AgNPs-PEG, the FTIR bands of NGO-AgNPs-PEG-DOX (Fig. 2) revealed characteristic modes of DOX molecules. The peak at 1638 cm^{-1} corresponds to the quinone group of DOX in drug loaded composite. In addition, the band assigned to C–H stretching was shifted from 2885 to 2879 cm^{-1} due to the methoxy group ($\text{CH}_3\text{--O}$) in that sample. In addition, increased intensity of the C–O vibration at 1640 cm^{-1} and emergence of the new bands at 1458 and 1351 cm^{-1} assigned to the N–H deformation mode of the amide bonds (amide II) indicates the covalent coupling and loading of DOX to nanocomposites. The band patterns at 1384 cm^{-1} and 667 cm^{-1} (below 1000 cm^{-1}) suggest the presence

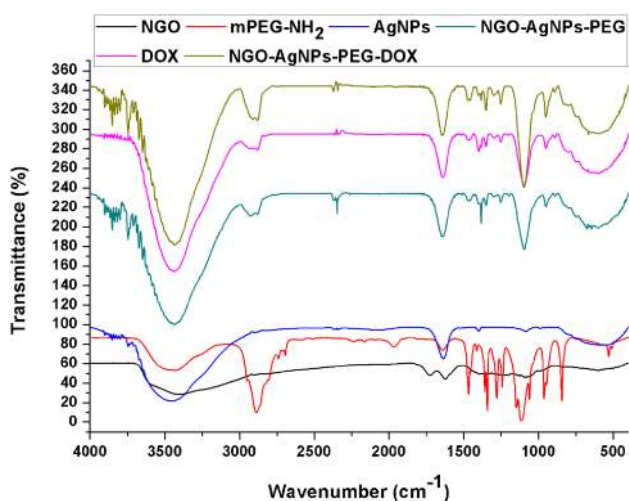


Fig. 2 Comparative FTIR-ATR spectra of pure NGO; mPEG-NH₂; AgNPs; NGO-AgNPs-PEG; DOX; and NGO-AgNPs-PEG-DOX

of AgNPs in the nanocomposites. Another peak can be assigned at 1096 cm^{-1} corresponds to C–N vibration of the amine groups on mPEG-NH₂ [36]. These characteristics indicate the surface embarking of NGO-AgNPs and DOX was successfully and abundantly incorporated onto NGO-AgNPs-PEG.

The morphologies of the produced NGO, AgNPs and NGO-AgNPs nanocomposites were characterized by FESEM (Fig. 3). The GO shows highly wrinkled morphology because of the oxygenated functional groups on the surface (Fig. 3a). This indicates the formation of well exfoliated NGO. Furthermore, pure cerium nanoparticles show more agglomeration (Fig. 3b). The partial reduction of GO to RGO in RGO-AgNPs led to a smoother surface, possibly due to the removal of oxygen containing groups. It is of importance to note that the AgNPs (indicated by large no of white spots) are immobilized on the surface of RGO (Fig. 3c, d). Actually, these white dots are deposited and well-dispersed onto the surfaces of the RGO sheets. This distinct structure directly demonstrates the perfect assembly between AgNPs and the RGO sheets. Moreover, it has been proved that the aggregation of AgNPs inhibited by the strong adhesion and interaction between graphene sheets and AgNPs during synthesis of RGO-AgNPs [31, 50].

Smart phase mapping image of NGO-AgNPs by FESEM Energy Dispersive X-Ray (EDX) spectroscopy show the presence of only Carbon, oxygen and silver which proves the purity of the nanocomposites and oxidation of graphite layers (Fig. 3e). In addition, the elemental

analysis of the prepared NGO-AgNPs by using EDX spectrum indicates the presence of carbon (48.70%), oxygen (32.58%), silver (18.72%) and gold (gold peak was attributed gold coating on sample during analysis) (Fig. 3f). This information suggests that graphene was present in purified and partially oxidised form. Silver atoms (free from impurities) are adsorbed on the surface of the NGO sheet. The existence of O signals along with the Ag indicates the AgNPs are crowned by phytochemicals through oxygen atom. Few layers of graphene oxide are found from HRTEM micrographs of NGO. In addition, at several places on graphene oxide nanosheets wrinkles were prominent (Fig. 4a). These wrinkles were probably due to oxidation of carbon atoms during synthesis. The selected area of electron diffraction (SAED) patterns exhibit only one set of hexagonal diffraction pattern which suggests hexagonal lattice plane of NGO with high crystallinity (Fig. 4a) [51, 52].

Surface morphology and particle size of the AgNPs were ascertained using HRTEM. Most of the AgNPs were roughly circular in shape with smooth edges. The rings of SAED pattern reveal the single face-centered cubic (fcc) crystalline property of the spherical AgNPs with a preferential growth direction along the (110), (200), (220) and (311) XRD planes of silver (Fig. 4b). In accordance with the UV-Vis spectroscopic analysis, the TEM images demonstrate roughly spherical AgNPs are irregularly poly-dispersed on NGO (Fig. 4c). The strong signal of the silver atoms suggests the crystalline property of AgNPs. In

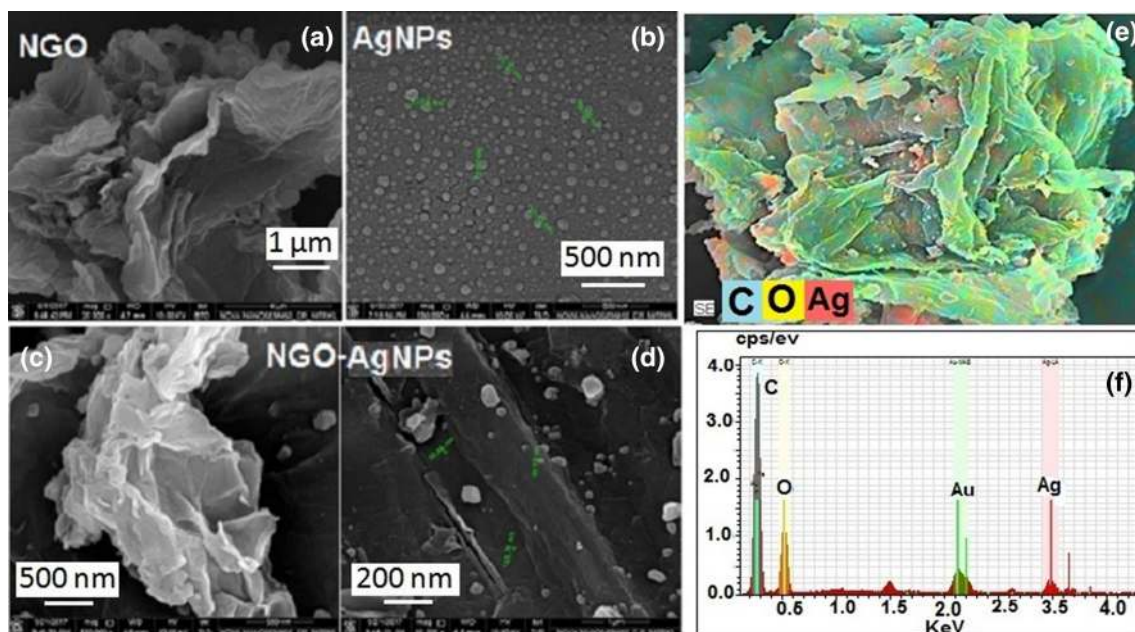
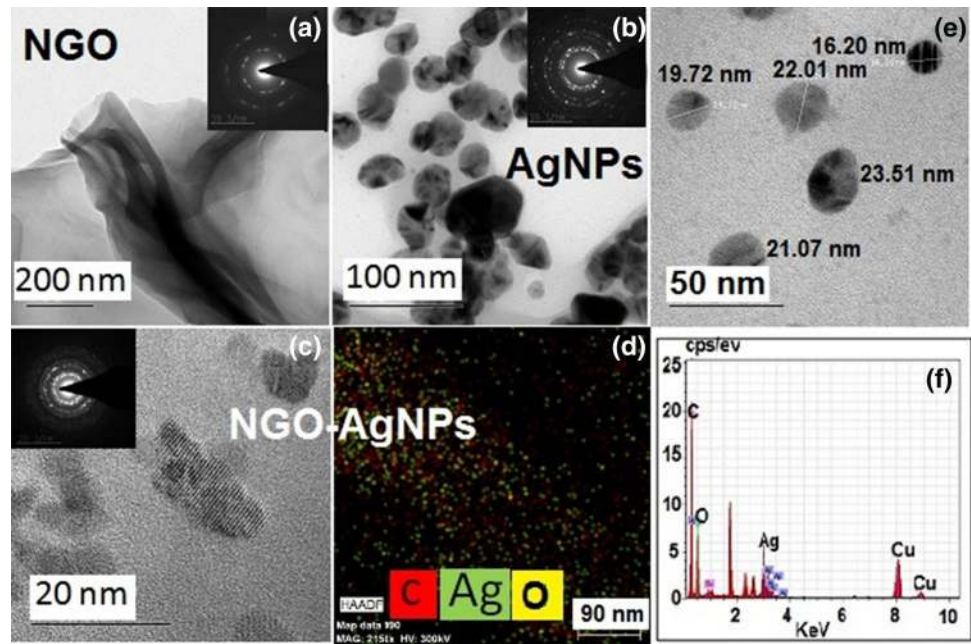


Fig. 3 FESEM images of **a** pure NGO showing exfoliation; **b** pure AgNPs with reduced agglomeration; **c**, **d** NGO-AgNPs showing dispersion of AgNPs on NGO sheet; **e** elemental mapping of NGO-

AgNPs showing elemental purity; and **f** energy dispersive X-ray (EDX) spectrum showed higher percentage of carbon signals along with oxygen and silver

Fig. 4 HRTEM images with their respective selected area electron diffraction (SAED) pattern of **a** pure NGO; **b** pure AgNPs; **c** NGO-AgNPs; **d** smart phase elemental mapping of NGO-AgNPs showing higher percentage of carbon signals along with oxygen and silver; **e** particle size of AgNPs dispersed on NGO sheet (less than 25 nm); **f** EDX spectrum of NGO-AgNPs showing more weight percentage of oxygen than silver



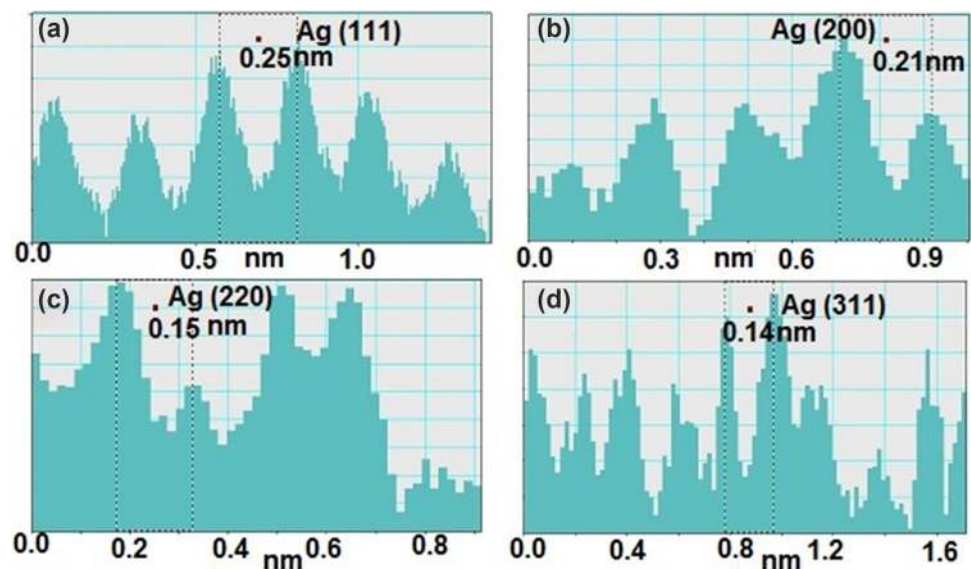
addition, finger printing and fringe patterns of AgNPs have been shown in Fig. 5.

The HRTEM images of NGO-AgNPs nanocomposites reveal that AgNPs are embedded on the surface of NGO (Fig. 4c). In addition, typical SAED pattern of NGO-AgNPs sample was used to study the crystalline nature of the AgNPs in the composite. The four visible diffraction rings are indexed as the crystal planes (111), (200), (220) and (311) of face-centered cubic (fcc) metallic Ag demonstrate multiple crystal diffraction features (Fig. 4c), which clearly confirms the presence of Ag nanoparticles in the nanocomposites. The findings corroborate the results of XRD analysis of pure AgNPs (Fig. 6) [40, 46]. Also similar to

FESEM results (Fig. 3f) the HRTEM EDX mapping image of NGO-AgNPs nanocomposite (Fig. 4d) confirms the presence of only carbon, oxygen and silver elements in it, which indicates successful formation of pure NGO-AgNPs nanocomposites [53]. Based on TEM analysis, it may be predicted that controlled particle size and uniform dispersion of AgNPs on graphene surface open a path for biomedical applications.

From the particle size analysis by HRTEM, it has been found that the pure AgNPs are agglomerated and larger in size (Fig. 4b) than the AgNPs on NGO (Fig. 4e). As demonstrated in Fig. 4e, most of the anchored AgNPs on NGO are very small (less than 25 nm). On the other hand, AgNPs

Fig. 5 Images of finger printing and fringe patterns by HRTEM, taken from a typical AgNPs in the NGO-AgNPs nanocomposites showing clear lattice fringes with an inter-plane distance measured as **a** 0.25 nm; **b** 0.21 nm; **c** 0.15 nm; and **d** 0.14 nm corresponding to the (111), (200), (220) and (311) planes of silver crystals, which corroborate the result of XRD analysis



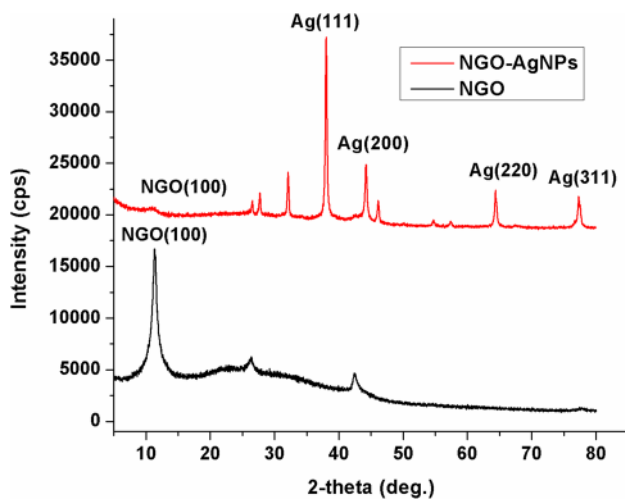


Fig. 6 Comparative XRD patterns of pure NGO showing (100) plane and NGO-AgNPs showing (100) plane for NGO; and (111), (200), (220) and (311) planes for AgNPs crystal lattice

synthesized without NGO was found to have an average size of 35 nm, and the particle size distribution suggested that most of them are above 30 nm. Hence, NGO has a vital role in the process of stabilization and formation of smaller AgNPs in the NGO-AgNPs nanocomposite [40]. EDX spectrum indicated that the presence of carbon, oxygen and silver elements were in NGO-AgNPs nanocomposites (Fig. 4f). Results showed that silver, oxygen, and carbon, contents (wt%) of NGO-AgNPs were 10.41%, 5.19%, and 84.41%, respectively. Like Chang et al., the NGO-AgNPs synthesized in the present study have also higher weight percentage of silver (both in EDX spectra of NGO-AgNPs FESEM and HRTEM analyses) this leads a conclusion that this syn-graphenization method of green synthesis is more reproducible [54]. Furthermore, the percentage of elements differs from the results of FESEM EDX analysis since AgNPs is polydispersed on NGO.

The XRD analysis is further used to confirm the formation of the NGO-AgNPs nanocomposites. The GO nanosheets exhibited a broad peak at 10.5° corresponding to the (100) plane with interlayer spacing of 0.84 nm, which indicates that the ordinal structures of graphite have been exploited and that oxygen-containing functional groups have been inserted into the interspaces.

However, in the XRD patterns of NGO-AgNPs, the disappeared diffraction pattern from GO suggests that Ag NPs are intercalated into stacked GO layers [33]. But one small broad peak at 10.97° having d-spacing of 0.80 nm was found, which may be due to the graphene nanosheet. This is indicative of the fact that graphene is partially reduced to reduced graphene (RGO) still some oxygen containing functionalities of GO are there [48]. Meanwhile, four prominent peaks located at 38.0° , 44.2° ,

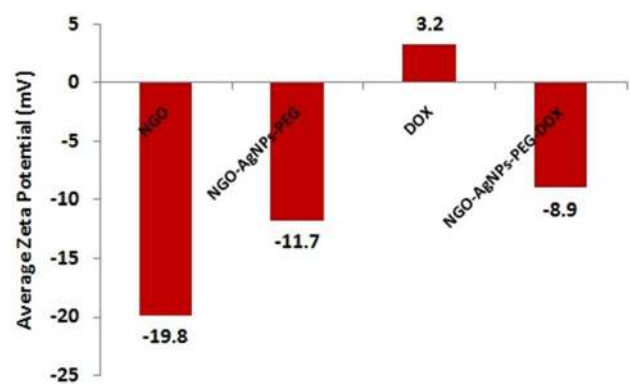


Fig. 7 Average values of zeta potential for NGO, NGO-AgNPs-PEG, DOX, and NGO-AgNPs-PEG-DOX

64.0° and 77.0° are ascribed to (111), (200), (220) and (311) crystallographic planes of face-centered cubic (fcc) crystal of Ag (JCPDS number 07–0783), respectively [55, 56]. These studies indicate that AgNPs are successfully decorated on the surface of NGO. The HRTEM image of a silver nanoparticle (Fig. 5) anchored to NGO, displays clear lattice fringes with interplane distances of 0.25, 0.21 and 0.15 and 0.14 nm corresponding to the (111), (200), (220) and (311) planes of silver crystals, which corroborate the result of XRD analysis (Fig. 6) (Table S2).

The electron diffraction rings, obtained from HRTEM SAED measurements as seen in Fig. 4a, represent (100) plane of NGO crystal lattice. The fringe widths measured from HRTEM at 5 nm resolution is exactly similar to the d-spacing values obtained from XRD pattern of NGO. It suggests the presence of graphitic regions within the NGO. But multiple electron diffraction rings, obtained from HRTEM SAED measurements as seen in Fig. 4b, represent (111), (200), (220) and (311) planes of AgNPs crystal lattice. HRTEM and XRD analyses demonstrated that the NGO, AgNPs, and NGO-AgNPs were synthesized using two-step process.

Zeta potential is an important criterion to determine the surface charge of nanocomposites that establishes the stability and absorption of nanocomposites at target site [57]. The conjugation of DOX with green synthesized NGO-AgNPs-PEG nanocomposites can further be interpreted by zeta potential measurement. The zeta potential value of NGO-AgNPs-PEG (-11.7 mV) was negative which was slightly increased after DOX loading (NGO-AgNPs-PEG-DOX: -8.9 mV) (Fig. 7) (Table S3). Due to the presence of NGO and AgNPs, zeta potential of the nanoformulation was negative. But free DOX was found to have positive zeta potential ($+3.2$ mV). So, the attachment of doxorubicin with NGO-AgNPs-PEG might be due to weak electrostatic attraction and dative bonding [7].

Because of the deprotonation of the functional moieties present on the GO, negative surface charge of the DOX loaded nanocomposites was found. It has been reported that typically, nanoformulations with negative zeta potential exhibit high degree of stability in physiological condition and enhanced brain tumor targeting by traversing the blood brain barrier [57, 58]. However, the positively charged nanocomposites favor protein adsorption to a larger extent, in case of free DOX, and it facilitates fast RES clearance [59]. Furthermore, negative charges on the surface of nanocomposite prevent the non specific absorption of nanocomposite on cells. Hence, the negative zeta potential value bypasses RES clearance and renders maximum circulation time to attain optimum enhanced permeability and retention (EPR) effect [60]. The EPR effect might be the main cause of more accumulation of nanocomposites in cancer cells leading to better efficacy of the loaded anticancer drug.

3.2 In vitro studies

3.2.1 Drug entrapment efficiency (%EE) and drug loading content (%DLC)

In order to assess the potential of NGO-AgNPs-PEG as controlled and targeted drug delivery systems, the potential of NGO-AgNPs-PEG nanocomposites as drug carrier must be determined by their drug encapsulation and drug loading properties [19].

Graphene oxide is expected to have magnificent drug loading behavior due to large specific surface area. The drug encapsulation efficiency and drug loading capacity of the nanocomposites were ascertained by determining the concentration of unbound drug using UV-Vis spectroscopy. In the present study, the formulations F_0 (10 $\mu\text{g/ml}$ of NGO), F_1 (1 $\mu\text{g/ml}$ of NGO-AgNPs-PEG), F_2 (10 $\mu\text{g/ml}$ of NGO-AgNPs-PEG), and F_3 (100 $\mu\text{g/ml}$ of NGO-AgNPs-PEG) were subjected to drug encapsulation efficiency and drug loading capacity studies. For F_0 , F_1 , F_2 , and F_3 , the percentage drug encapsulation was 70%, 42%, 73%, and 79%, respectively, while their corresponding values of percentage drug loading were 198%, 194%, 218%, and 73% (Table S4). By increasing the proportions of NGO-AgNPs-PEG nanocomposites (from 1 to 10 $\mu\text{g/ml}$) in F_1 and F_2 , keeping drug input constant (the amount of drug dissolved in the aqueous phase during nanocomposite preparation was 50 $\mu\text{g/ml}$), the values of both percentage drug encapsulation and percentage drug loading were increased (Table S4). However, when nanocomposite input was raised from 10 to 100 $\mu\text{g/ml}$ (in cases of F_2 and F_3), keeping the amount of drug constant (50 $\mu\text{g/ml}$), the %loading was decreased (from 218 to 73%). This anomaly, in case of %loading, may be due to increase in total solids

feed in F_3 . In addition to the amount of solids feed in the formulation, framework structure and architecture (pore geometry) of NGO also affect the drug loading percentage [23]. Moreover, the highly mesoporous nature of NGO having large pore surface area may provide a good platform for better drug loading up to 218%.

In this connection, it may be mentioned that according to some researchers, pure GO can load DOX with the loading capacity up to 192%, implying GO was appeared to have a greater potency for DOX loading [29]. On the other hand, at the very moment DOX was loaded, DOX loaded GO sheets showed more aggregation. But, the GO modified with PEG and lactobionic acid by EDC-NHS chemistry exhibited potency for DOX loading up to 85% [61]. Simultaneously, PEGylated green synthesised silver nanocomposites can load DOX up to 87% [7]. On the other hand, in the present study design, the NGO-AgNPs-PEG-DOX nanocomposites produced by EDC-NHS chemistry appeared to show synergistic drug loading up to 218%.

On the other hand, percentage drug encapsulation depends on relative proportions of nanocomposite to drug in different formulations. So, its values were increased gradually from F_1 to F_3 . Considering the above mentioned reasons, F_2 exhibited much higher loading in the nanocomposites than F_1 and F_3 , whereas the value of %drug encapsulation was maximum in case of F_3 .

In this connection, it may be mentioned that the drug loading and encapsulation in the NGO-AgNPs-PEG nanocomposites are appeared to be governed by the partitioning of the drug between the PEGylated nanocomposites matrix phase and the external aqueous phase [62], while considering the drug efficacy, loading efficiency is more vital than encapsulation efficiency. So, out of three formulations F_2 was initially selected.

Prior to surface modification, the surfaces of GO had a large number of hydroxyl and carboxyl groups, and the interaction between graphene oxide and drug was mainly formed between hydroxyl and carboxyl groups. After amino modification, the oxygen containing groups on the surface of GO reduced while the number of amino groups increased. Since PEGylated nanocomposites showed more loading capacity than pure NGO (mentioned earlier), it seems that the hydrogen bonding forces formed between amino groups of NGO-AgNPs-PEG and DOX were stronger than those between pure NGO and DOX. That may be the reason why the amino modified NGO-AgNPs-PEG facilitated more drug loading capacity than pure NGO [63].

The overall results suggest that the positively charged DOX molecules (in three formulations) were more easily loaded onto the surfaces of GO based nanocarrier with lower zeta potentials (mentioned earlier), indicating that electrochemical interactions as well as attractive non-covalent (π - π stacking) interactions also play a vital role

in DOX loading. As a result, this nanocomposite can exhibit ultra-high DOX loading capacity and efficiency compared with many other common nano cargoes [19, 64–66]. Therefore, this graphene based charge-reversal nano cargo is a potential vehicle for more effective loading and delivery of DOX.

3.2.2 Drug release response

The in vitro drug release studies of F_0 , F_1 , F_2 , and F_3 were carried out both in phosphate buffer (pH 7.4) and in acidic buffer (pH 5.4). After 7, 13 and 24 h, in phosphate buffer, drug release was found to be 32.5%, 35.10% and 37.70%, respectively, from formulation F_0 ; 26.5%, 27.10% and 27.70%, respectively, from formulation F_1 ; 17.3%, 18.20% and 18.60% in case of formulation F_2 ; and 15.40%, 16.30% and 16.6% from formulation F_3 , whereas corresponding release values were 75.3%, 84.6% and 90.1% from formulation F_0 ; 43.2%, 55.3.4% and 65.4% from formulation F_1 ; 63%, 72% and 79% in case of formulation F_2 ; and 60.4%, 69.5% and 76.1% from formulation F_3 when acidic buffer was used. So, all formulations showed slower drug release rate in phosphate buffer (Table S5). In cases of both the buffers, an initial burst release was observed for the drug during the first 7 h and followed by controlled release up to 120 h (Fig. 8). Moreover, maximum drug release rate was between 5 and 7 h in phosphate buffer (Fig. 8a), while in acidic buffer it was between 9 and 11 h (Fig. 8b), which favored controlled and targeted drug release. Along with this, larger values of standard deviation and variance of data relating to the drug release profile in acidic buffer as compared to in phosphate buffer signify more spreadability and controlled release of the drug in acidic buffer.

Both NGO-DOX and NGO-AgNPs-PEG-DOX exhibited significant controlled release. The acidic pH of the solution might trigger DOX release by weakening the hydrogen bonds between DOX and GO (–OH and –COOH), reducing the non-covalent interactions and hydrogen bonding. Furthermore, NGO-AgNPs-PEG-DOX was able to have higher and controlled DOX release than NGO-DOX, as the release of DOX from NGO-DOX was not so pH controlled as from the charge-reversal PEGylated GO [61]. Hence, as acidic environment favors higher and controlled DOX release from NGO-AgNPs-PEG-DOX, the micro-environments of cancerous tissues, which have low pH as well as the presence of intracellular lysosomes or endosomes, trigger drug release at the targeted cancerous tissues.

DOX is a weak amphipathic base with $pK_a=8.3$. There is an electrostatic interaction between amino group of DOX and the carboxylic acid moieties on the NGO-AgNPs-PEG surface due to their carboxylate form (pK_a range 3–5) at physiological pH (7.4) [67]. Thus, the electrostatic interactions between DOX molecules and NGO-AgNPs-PEG

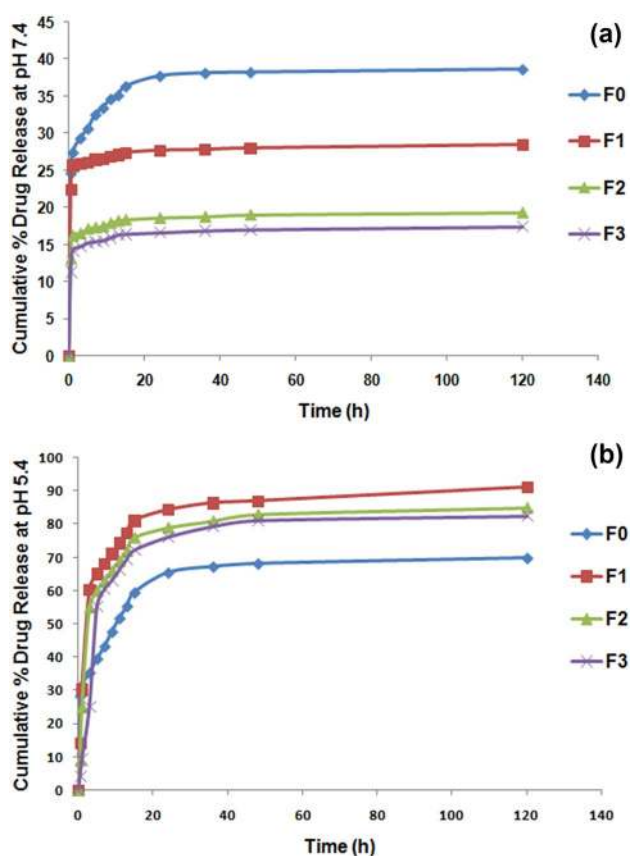


Fig. 8 Cumulative percentage DOX release from F_0 (10 $\mu\text{g/ml}$ of NGO); F_1 (1 $\mu\text{g/ml}$ of NGO-AgNPs-PEG); F_2 (10 $\mu\text{g/ml}$ of NGO-AgNPs-PEG); F_3 (100 $\mu\text{g/ml}$ of NGO-AgNPs-PEG) in **a** pH 7.4 phosphate buffer and **b** pH 5.4 acidic buffer

nanocomposite remain unaltered at physiological pH. This indicates that the NGO-AgNPs-PEG nanocomposites may contribute to an extended circulation of DOX and thus an improvement in therapeutic efficacy with reduction of adverse drug reaction of free DOX [68].

On the other hand, at pH 5.4, the electrostatic interactions between NGO-AgNPs-PEG nanocomposite and protonated DOX were reduced, and weakening of hydrogen bonds between them lead to the higher rate and extent of targeted drug release [67]. Thus, the percentage of drug release rate is negatively correlated with the pH, which is useful for targeted drug release.

In summary, the type of bonding and chemical interaction between NGO-AgNPs-PEG and DOX and dissolution of DOX from pores of nanocomposite may be liable for controlled release of DOX from NGO-AgNPs-PEG nano platform. The knowledge obtained from the findings of Huang et al. suggests that the pH-sensitive DOX release could open the door for NGO-AgNPs-PEG to release its drug in the acidic pH environment of cancer cells in addition to enhanced cytotoxicity [68]. Considering all the

above mentioned information, it may be concluded that the elevated drug loading and more pH-guided release of DOX from NGO-AgNPs-PEG could be possible. Thus, NGO-AgNPs-PEG may be considered as an encouraging drug delivery vehicle for the anti-malignant drug DOX. To know about the efficacy of NGO-AgNPs-PEG as a delivery vehicle, cell culture experiment was also performed. The results of that study have been mentioned in the later part of this article.

3.2.3 Release kinetics

The greater values of regression coefficient suggest that all dosage forms of DOX in both alkaline and acidic buffer followed Korsmeyer–Peppas model release kinetics.

While the regression coefficient values for F_0 , F_1 , F_2 , and F_3 and their corresponding 'n' values for Korsmeyer–Peppas model indicate their quasi Fickian release in phosphate buffer, whereas their regression coefficient values and their corresponding 'n' values for Korsmeyer–Peppas model suggest quasi Fickian release except F_3 which showed anomalous non-Fickian release in acidic buffer (Table S6). Although drug release is more likely to be diffusion driven, which is associated with concentration gradient and the degree of swelling of PEG [28, 69], in cases of F_3 , the drug release may be controlled by both diffusion and polymer relaxation in acidic buffer (considering the above mentioned results).

The values of dissimilarity (f_1) and similarity (f_2) factors (according to the model independent method) for comparison of drug release pattern from F_0 and F_2 were found to be 32.07 which was more than 15 and 38.8 was less than 50, respectively, in acidic buffer, whereas their corresponding values were 47.81 which was more than 15 and 39.35 was less than 50 in phosphate buffer. Considering the values of f_1 and f_2 , it might be ensured that the release profiles (in both buffers) of F_0 – F_2 formulations of DOX were dissimilar. This result indicates that after surface functionalization of NGO the pattern of DOX release from NGO-AgNPs-PEG-DOX is different from NGO-DOX in both phosphate and acidic buffer. Considering the above mentioned information, it may be concluded that this smart NGO-CeNPs-PEG-DOX nanocomposite can be considered to be special, as it is selectively active only against cancerous tissue having acidic microenvironment.

3.3 Cytotoxicity study

The cell viability of normal cells cultured with GO may be enhanced by surface functionalization with a biocompatible polymer like PEG [19, 70, 71]. The silver nanoparticles by PEGylation [7] significantly improve the normal cell viability of the respective nanocomposites. Likewise,

the present data also indicate that PEG functionalized graphene nanosheets are biocompatible. Moreover, PEG could also act as a stabilizing agent, as earlier work showed that PEGylated GO was found to have more stability in systemic circulation than pure GO [72]. Considering these information, it is expected that when surface-treated with PEG, the functionalized NGO metal nanocomposites at a higher concentration may also be used as a drug carrier without incurring toxicity to cells.

It was found that on HaCaT cells, NGO, NGO-AgNPs and NGO-AgNPs-PEG nanocomposites, at a concentration of 10 $\mu\text{g/ml}$, showed cell viability of 75.12%, 61.18% and 70.28%, respectively, indicating enhancement of biocompatibility after PEGylation of graphene nanocomposites (Fig. 9a) (Table S7). However, pure AgNPs revealed prominent cytotoxic effect on HeLa cell lines. It was also found that AgNPs in NGO-AgNPs showed synergistic cytotoxic action on both HaCaT and HeLa cell lines. But after PEGylation biocompatibility of functionalized nanographene oxide containing AgNPs was enhanced to some extent (Fig. 9) (Table S7). From earlier investigation, it can be mentioned that surface modification of metal decorated NGO with this biocompatible polymer (PEG) may lower the reactive oxygen species effect on normal cells and modifies its cellular uptake [72], which may reduce the cytotoxic effect on HaCaT cells treated with PEGylated metal decorated NGO [73]. So, it is expected that NGO-AgNPs-PEG may increase the cell viability of HaCaT cell lines. The cell

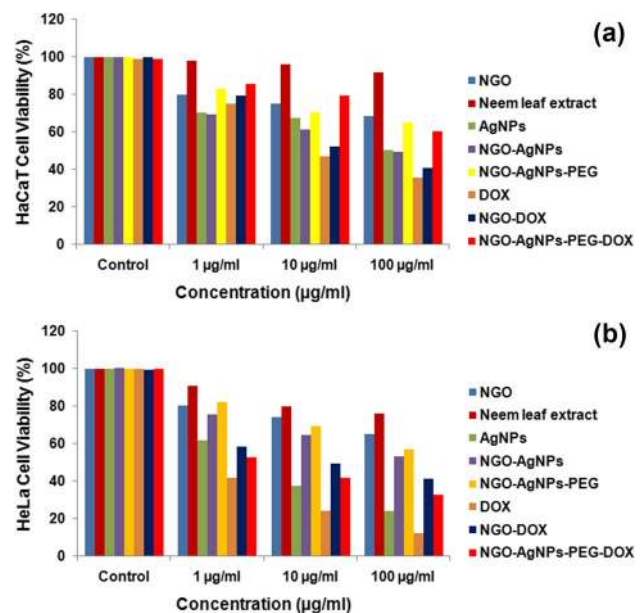


Fig. 9 Cytotoxicity Study (after 48 h incubation) of NGO; neem leaf extract; AgNPs; NGO-AgNPs; NGO-AgNPs-PEG; Pure DOX; NGO-DOX; and NGO-AgNPs-PEG-DOX at different concentrations (1 $\mu\text{g/ml}$, 10 $\mu\text{g/ml}$ and 100 $\mu\text{g/ml}$) of each sample on cell viability (% of control) **a** using HaCaT cell line; **b** in case of HeLa cell line

viability on both HaCaT and HeLa cell lines indicates that the silver decorated nanographene oxide (below 10 µg/ml) can only be used as a targeted drug carrier (Table S7). The aqueous leaf extract of neem is biocompatible but it has some cytotoxic effect on HeLa cell lines which favor its use in synthesis of AgNPs.

Cytotoxic property of various DOX loaded graphene nano cargos along with pure DOX at different concentrations were studied on both HaCaT and HeLa cell lines. Various samples of DOX (mentioned earlier) at different concentrations (1 µg/ml, 10 µg/ml and 100 µg/ml) were injected separately into both the cell lines to measure cell viability after 48 h incubation. Against the above mentioned trend, Fig. 10 shows that DOX loaded PEGylated functionalized silver decorated nanographene oxide were more cytotoxic as compared to NGO-DOX. That may be due to effective and controlled release of DOX from the NGO-AgNPs-PEG-DOX nanocomposite than from the NGO-DOX. Furthermore, it was also revealed that the drug loaded targeted nano carrier, in the forms of NGO-AgNPs-PEG-DOX had greater cytotoxicity than did the nontargeting one, which suggests the potential of selective internalization, cellular uptake and lethality towards specific cancer cells (results obtained from phase contrast microscopic image analysis) for the targeting drug carrier (Fig. 10). From Fig. 9b, it is also clear that free DOX has a potent cytotoxic effect on HeLa cell line. Since free DOX cannot differentiate between normal cells and tumour cells, it might produce side effects during treatment of

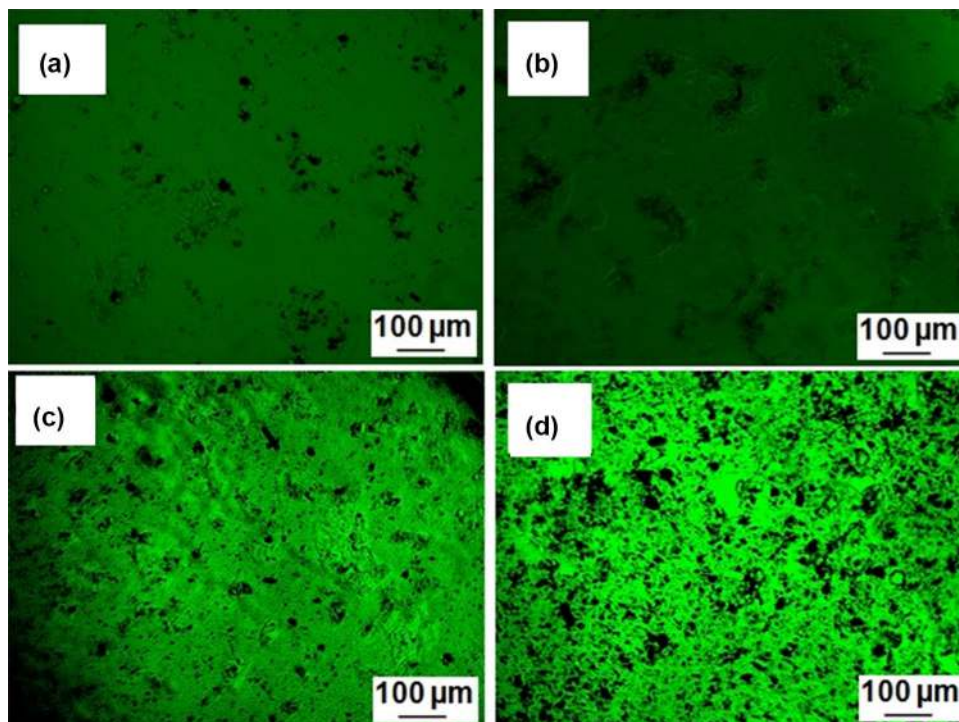
cancer. Accordingly, on HaCaT cell lines, the cytotoxicity study results indicate DOX-loaded PEGylated silver decorated graphene nanocomposite, as compared to free DOX, had lesser harmful effect on normal cell than cancer cells. So, that nanocomposite may be preferred over free DOX although its cell killing effect is comparatively low.

It seems that RGO-AgNPs-PEG may be favourable vehicle in anti-cancer drug delivery with optimum circulation self life, EPR effect that would up-regulate intratumoral drug delivery due to greater permeability of tumor vasculatures, and multivalent effect [74]. So, it may be concluded that targeted drug carriers of PEGylated silver activated functionalized nanographene oxide could bypass the side effects of free DOX in tumor therapy. Furthermore, for better understanding, a conceptual overview of this strategy is provided by the schematic diagram shown in Scheme 1.

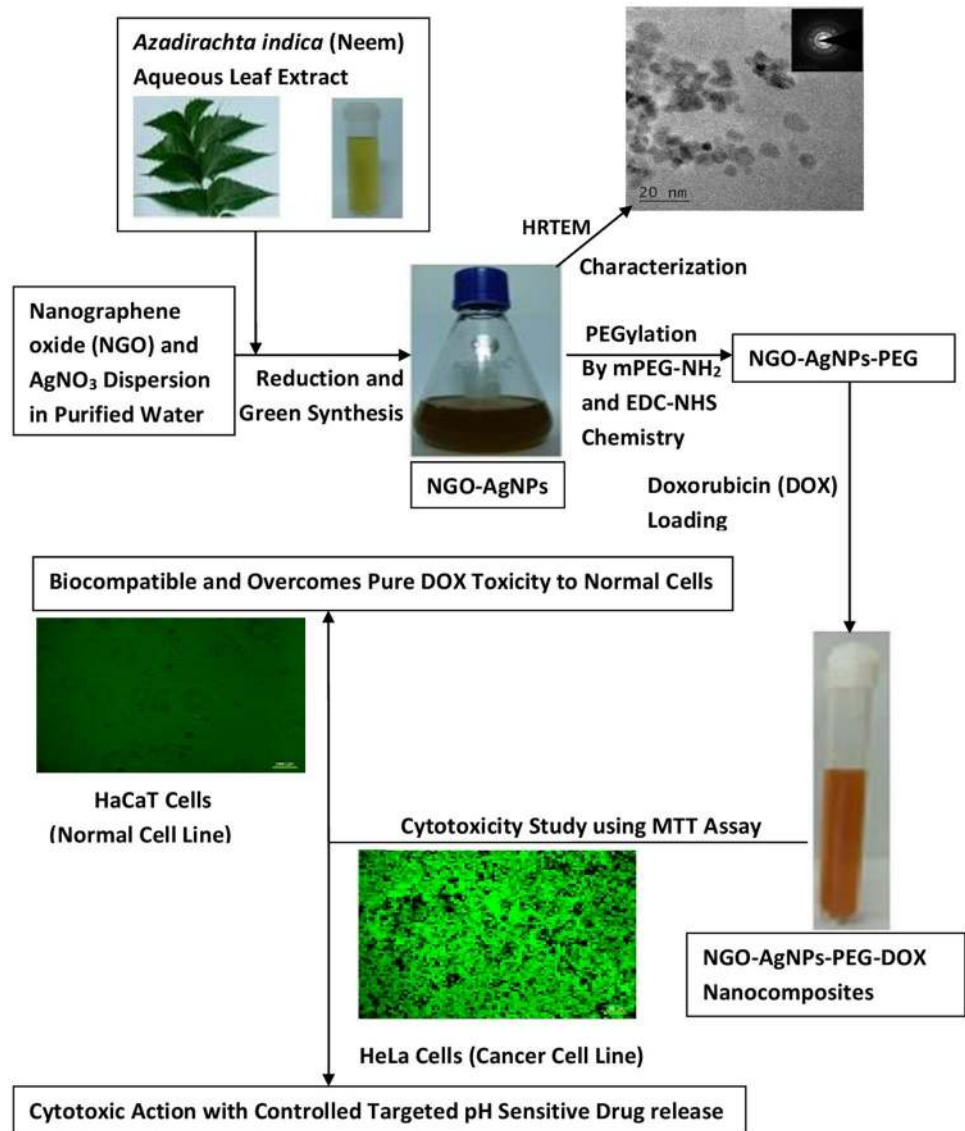
4 Conclusion

This study design demonstrated a green chemistry approach for the synthesis of PEGylated silver decorated graphene nanoplatfrom at ambient reaction conditions using '*Azadirachta indica* (*A. indica*)' aqueous leaf extract. The leaf extract acts as a reducing, stabilizing/capping and anticancer agent. The green chemistry approach is eco-friendly and non-toxic. To get rid of toxic gases and some impurities, Modified Hummers Method was further

Fig. 10 Phase contrast microscopic images of HaCaT normal cell lines incubated with **a** 10, and **b** 100 µg/ml NGO-AgNPs-PEG-DOX for 48 h, after MTT treatment. Phase contrast microscopic images of HeLa cancer cell lines incubated with **c** 10, and **d** 100 µg/ml NGO-AgNPs-PEG-DOX for 48 h, after MTT treatment [cytoplasm of viable cells showing intense green fluorescence and dead cells showing no fluorescence (black in colour)]



Scheme 1 Overall schematic representation for the green synthesis, characterization of biosynthesized DOX loaded PEGylated NGO-AgNPs and their probable applications in controlled targeted drug delivery



modified for the synthesis of nano-graphene (NGO). As we know, graphene has the unique ability in the attachment and delivery of aromatic, water insoluble drugs. NGO-PEG renders high aqueous solubility and stability in physiological solutions. Silver NPs possess significant toxicity to cancer cells via the induction of apoptosis whereas normal immune system cells are almost unaffected. Formation of nanocomposite was confirmed by different analytical techniques and even the elemental purity of the nanocomposite was assured by performing the elemental analysis of the synthesized nanocomposite. Thus obtained nanocomposite consists of silver nanoparticles with the size of ~25 nm uniformly decorated on the NGO sheets, which could prevent the agglomeration of the AgNPs and open a path for biomedical applications. In addition, negative zeta potential on the surface of nanocomposite prevents the non specific absorption of nanocomposite

on cells. The formed Smart pH stimuli responded NGO-AgNPs-PEG-DOX nanopatform exhibits non-compromised therapeutic efficacy when compared with free DOX while considering the side effect of free drug on normal cells. Importantly, the multifunctional NGO-AgNPs-PEG-DOX is able to specifically target cancer cells, and exert specific cytotoxic effect against the cancer cells. Considering the above mentioned information it may be concluded that the developed NGO-AgNPs-PEG nano-carrier may hold a great promise to be used for targeted and controlled drug delivery in tumor therapy.

Compliance with ethical standards

Conflict of interest All authors declare that they have no conflict of interest.

References

1. Zhang W, Guo Z, Huang D, Liu Z, Guo X, Zhong H (2011) Synergistic effect of chemo-photothermal therapy using PEGylated graphene oxide. *Biomaterials* 32:8555–8561. <https://doi.org/10.1016/j.biomaterials.2011.07.071>
2. Knop K, Hoogenboom R, Fischer D, Schubert US (2010) Poly(ethylene glycol) in drug delivery: pros and cons as well as potential alternatives. *Angew Chem Int Ed Engl* 49:6288–6308. <https://doi.org/10.1002/anie.200902672>
3. Akhavan O, Ghaderi E, Aghayee S, Fereydooni Y, Talebi A (2012) The use of a glucose reduced graphene oxide suspension for photothermal cancer therapy. *J Mater Chem* 22:13773–13781. <https://doi.org/10.1039/C2JM31396K>
4. Mukherjee S, Chowdhury D, Kotcherlakota R, Patra S, Vinothkumar B, Bhadra MP, Sreedhar B, Patra CR (2014) Potential theranostics application of biosynthesized silver nanoparticles (4-in-1 system). *Theranostics* 4:316–335. <https://doi.org/10.7150/thno.7819>
5. Poliakov M, Licence P (2007) Sustainable technology: green chemistry. *Nature* 450:810–812. <https://doi.org/10.1038/450810a>
6. Mukherjee S, Vinothkumar B, Prashanthi S, Bangal PR, Sreedhar B, Patra CR (2013) Potential therapeutic and diagnostic applications of one-step in situ biosynthesized gold nanoconjugates (2-in-1 system) in cancer treatment. *RSC Adv* 3:2318–2329. <https://doi.org/10.1039/C2RA22299J>
7. Patra S, Mukherjee S, Barui AK, Ganguly A, Sreedhar B, Patra CR (2015) Green synthesis, characterization of gold and silver nanoparticles and their potential application for cancer therapeutics. *Mater Sci Eng, C* 53:298–309. <https://doi.org/10.1016/j.msec.2015.04.048>
8. Patel SM, Venkata KCN, Bhattacharyya P, Sethi G, Bishayee A (2016) Potential of neem (*Azadirachta indica* L.) for prevention and treatment of oncologic diseases. *Semin Cancer Biol* 40–41:100–115. <https://doi.org/10.1016/j.semcan.2016.03.002>
9. Harish Kumar GK, Vidya Priyadarsini R, Vinothini G, Vidjaya Letchoumy P, Nagini S (2010) The neem limonoids azadirachtin and nimbolide inhibit cell proliferation and induce apoptosis in an animal model of oral oncogenesis. *Investig New Drugs* 28:392–401. <https://doi.org/10.1007/s10637-009-9263-3>
10. Hao F, Kumar S, Yadav N, Chandra D (2014) Neem components as potential agents for cancer prevention and treatment. *Biochim Biophys Acta* 1846:247–257. <https://doi.org/10.1016/j.bbcan.2014.07.002>
11. Singh V, Joung D, Zhai L, Das S, Khondaker SI, Seal S (2011) Graphene based materials: past, present and future. *Prog Mater Sci* 56:1178–1271. <https://doi.org/10.1016/j.pmatsci.2011.03.003>
12. Wang H, Robinson JT, Diankov G, Dai H (2010) Nanocrystal growth on graphene with various degrees of oxidation. *J Am Chem Soc* 132:3270–3271. <https://doi.org/10.1021/ja100329d>
13. Liang Y, Wang H, Sanchez CH, Chen Z, Dai H (2010) TiO₂ nanocrystals grown on graphene as advanced photocatalytic hybrid materials. *Nano Res* 3:701–705. <https://doi.org/10.1007/s12274-010-0033-5>
14. Zhou X, Huang X, Qi X, Wu S, Xue C, Boey FYC, Yan Q, Chen P, Zhang H (2009) In situ synthesis of metal nanoparticles on single-layer graphene oxide and reduced graphene oxide surfaces. *J Phys Chem C* 113:10842–10846. <https://doi.org/10.1021/jp903821n>
15. Herrera-Alonso M, Abdala AA, McAllister MJ, Aksay IA, Prud'homme RK (2007) Intercalation and stitching of graphite oxide with diaminoalkanes. *Langmuir* 23:10644–10649. <https://doi.org/10.1021/la0633839>
16. Stankovich S, Piner RD, Chen XQ, Wu NQ, Nguyen ST, Ruoff RS (2006) Stable aqueous dispersions of graphitic nanoplatelets via the reduction of exfoliated graphite oxide in the presence of poly(sodium 4-styrenesulfonate). *J Mater Chem* 16:155–158. <https://doi.org/10.1039/B512799H>
17. Stankovich S, Piner RD, Nguyen ST, Ruoff RS (2006) Synthesis and exfoliation of isocyanate-treated graphene oxide nanoplatelets. *Carbon* 44:3342–3347. <https://doi.org/10.1016/j.carbon.2006.06.004>
18. Liu Z, Robinson JT, Sun X, Dai H (2008) PEGylated nanographene oxide for delivery of water-insoluble cancer drugs. *J Am Chem Soc* 130:10876–10877. <https://doi.org/10.1021/ja803688x>
19. Zhou T, Zhou X, Xing D (2014) Controlled release of doxorubicin from graphene oxide based charge-reversal nanocarrier. *Biomaterials* 35:4185–4194. <https://doi.org/10.1016/j.biomaterials.2014.01.044>
20. Aggarwal P, Hall JB, McLeland CB, Dobrovolskaia MA, McNeil SE (2009) Nanoparticle interaction with plasma proteins as it relates to particle biodistribution, biocompatibility and therapeutic efficacy. *Adv Drug Deliv Rev* 61:428–437. <https://doi.org/10.1016/j.addr.2009.03.009>
21. Petersen H, Fechner PM, Fischer D, Kissel T (2002) Synthesis, characterization, and biocompatibility of polyethylenimine-graft-poly(ethylene glycol) block copolymers. *Macromolecules* 35:6867–6874. <https://doi.org/10.1021/ma012060a>
22. Pasut G, Veronese FM (2007) Polymer-drug conjugation, recent achievements and general strategies. *Prog Polym Sci* 32:933–961. <https://doi.org/10.1016/j.progpolymsci.2007.05.008>
23. Ardeshirzadeh B, Anaraki NA, Irani M, Rad LR, Shamshiri S (2015) Controlled release of doxorubicin from electrospun PEO/chitosan/graphene oxide nanocomposite nanofibrous scaffolds. *Mater Sci Eng C Mater Biol Appl* 48:384–390. <https://doi.org/10.1016/j.msec.2014.12.039>
24. Rana VK, Choi MC, Kong JY, Kim GY, Kim MJ, Kim SH, Mishra S, Singh RP, Ha CS (2011) Synthesis and drug-delivery behavior of chitosan-functionalized graphene oxide hybrid nanosheets. *Macromol Mater Eng* 296:131–140. <https://doi.org/10.1002/mame.201000307>
25. Zhang L, Xia J, Zhao Q, Liu L, Zhang Z (2010) Functional graphene oxide as a nanocarrier for controlled loading and targeted delivery of mixed anticancer drugs. *Small* 6:537–544. <https://doi.org/10.1002/sml.200901680>
26. Simoes S, Moreira JN, Fonseca C, Düzgüneş N, de Lima MCP (2004) On the formulation of pH-sensitive liposomes with long circulation times. *Adv Drug Deliv Rev* 56:947–965. <https://doi.org/10.1016/j.addr.2003.10.038>
27. Felber AE, Dufresne MH, Leroux JC (2012) pH-sensitive vesicles, polymeric micelles, and nanospheres prepared with polycarboxylates. *Adv Drug Deliv Rev* 64:979–992. <https://doi.org/10.1016/j.addr.2011.09.006>
28. Huang YS, Lu YJ, Chen JP (2017) Magnetic graphene oxide as a carrier for targeted delivery of chemotherapy drugs in cancer therapy. *J Magn Magn Mater* 427:34–40. <https://doi.org/10.1016/j.jmmm.2016.10.042>
29. Lei H, Xie M, Zhao Y, Zhang F, Xu Y, Xie J (2016) Chitosan/sodium alginate modified graphene oxide-based nanocomposite as a carrier for drug delivery. *Ceram Int* 42:17798–17805. <https://doi.org/10.1016/j.ceramint.2016.08.108>
30. Zhang S, Yang K, Feng LZ, Liu Z (2011) In vitro and in vivo behaviors of dextran functionalized graphene. *Carbon* 49:4040–4049. <https://doi.org/10.1016/j.carbon.2011.05.056>
31. Zahed B, Hosseini-Monfared H (2015) A comparative study of silver-graphene oxide nanocomposites as a recyclable catalyst for the aerobic oxidation of benzyl alcohol: support effect. *Appl Surf Sci* 328:536–547. <https://doi.org/10.1016/j.apsusc.2014.12.078>

32. Das MR, Sarma RK, Borah SC, Kumari R, Saikia R, Deshmukh AB, Shelke MV, Sengupta P, Szunerits S, Boukherroub R (2013) The synthesis of citrate-modified silver nanoparticles in an aqueous suspension of graphene oxide nanosheets and their antibacterial activity. *Colloids Surf B Biointerfaces* 105:128–136. <https://doi.org/10.1016/j.colsurfb.2012.12.033>
33. Li YM, Chang XP, Cheng YJ, Chen S, He F, Zhuo RX (2017) Mercaptan acids modified amphiphilic copolymers for efficient loading and release of doxorubicin. *Colloids Surf B Biointerfaces* 153:220–228. <https://doi.org/10.1016/j.colsurfb.2017.02.022>
34. Sasikala ARK, Thomas RG, Unnithan AR, Saravanakumar B, Jeong YY, Park CH, Kim CS (2016) Multifunctional nanocarpets for cancer theranostics: remotely controlled graphene nanoheaters for thermo-chemosensitisation and magnetic resonance imaging. *Sci Rep* 6:20543. <https://doi.org/10.1038/srep20543>
35. El-Hamshary H, El-Newehy MH, Abdulhameed MM, El-Faham A, Elsherbiny AS (2019) Evaluation of clay-ionene nanocomposite carriers for controlled drug delivery: synthesis, in vitro drug release, and kinetics. *Mater Chem Phys* 225:122–132. <https://doi.org/10.1016/j.matchemphys.2018.12.054>
36. Siriviriyanun Popova M, Imae T, Kiew LV, Looi CY, Wong WF, Lee HB, Chung LY (2015) Preparation of graphene oxide/dendrimer hybrid carriers for delivery of doxorubicin. *Chem Eng J* 281:771–781. <https://doi.org/10.1016/j.cej.2015.07.024>
37. Cuong TV, Pham VH, Hahn SH, Chung JS, Shin EW, Kim EW (2010) Photoluminescence and raman studies of graphene thin films prepared by reduction of graphene oxide. *Mater Lett* 64:399–401. <https://doi.org/10.1016/j.matlet.2009.11.029>
38. Wang CC, Luconi MO, Masi AN, Fernández LP (2009) Derivatized silver nanoparticles as sensor for ultra-trace nitrate determination based on light scattering phenomenon. *Talanta* 77:1238–1243. <https://doi.org/10.1016/j.talanta.2008.08.035>
39. Gurunathan S, Han JW, Eppakayala V, Kim JH (2013) Microbial reduction of graphene oxide by *Escherichia coli*: a green chemistry approach. *Colloids Surf B Biointerfaces* 102:772–777. <https://doi.org/10.1016/j.colsurfb.2012.09.011>
40. de Faria AF, Martinez DST, Meira SMM, de Moraes ACM, Brandelli A, Filho AGS, Alves OL (2014) Anti-adhesion and antibacterial activity of silver nanoparticlessupported on graphene oxide sheets. *Colloids Surf B Biointerfaces* 113:115–124. <https://doi.org/10.1016/j.colsurfb.2013.08.006>
41. Vatanpour V, Shokravi A, Zarrabi H, Nikjavan Z, Javadi A (2015) Fabrication and characterization of anti-fouling and antibacterial Ag-loaded graphene oxide/polyethersulfone mixed matrix membrane. *J Ind Eng Chem* 30:342–352. <https://doi.org/10.1016/j.jiec.2015.06.004>
42. Xu Y, Liu Z, Zhang X, Wang Y, Tian J, Huang Y, Ma Y, Zhang X, Chen Y (2009) A graphene hybrid material covalently functionalized with porphyrin: synthesis and optical limiting property. *Adv Mater* 21:1275–1279. <https://doi.org/10.1002/adma.200801617>
43. Shen J, Shi M, Yan B, Ma H, Li N, Hu Y, Ye M (2010) Covalent attaching protein to graphene oxide via diimide-activated amidation. *Colloids Surf B Biointerfaces* 82:434–438. <https://doi.org/10.1016/j.colsurfb.2010.07.035>
44. Shan C, Yang H, Han D, Zhang Q, Ivaska A, Niu L (2009) Water-soluble graphene covalently functionalized by biocompatible poly-L-lysine. *Langmuir* 25:12030–12033. <https://doi.org/10.1021/la903265p>
45. Dreyer DR, Park S, Bielawski CW, Ruoff RS (2010) The chemistry of graphene oxide. *Chem Soc Rev* 39:228–240. <https://doi.org/10.1039/B917103G>
46. Bao Q, Zhang D, Qi P (2011) Synthesis and characterization of silver nanoparticle and graphene oxide nanosheet composites as a bactericidal agent for water disinfection. *J Colloid Interface Sci* 360:463–470. <https://doi.org/10.1016/j.jcis.2011.05.009>
47. Oh J, Lee JH, Koo JC, Choi HR, Lee Y, Kim T, Luong ND, Nam JD (2010) Graphene oxide porous paper from amine-functionalized poly(glycidyl methacrylate)/graphene oxide core-shell microspheres. *J Mater Chem* 20:9200–9204. <https://doi.org/10.1039/C0JM00107D>
48. Gu D, Chang X, Zhai X, Sun S, Li Z, Liu T, Dong L, Yin Y (2016) Efficient synthesis of silver-reduced graphene oxide composites with prolonged antibacterial effects. *Ceram Int* 42:9769–9778. <https://doi.org/10.1016/j.ceramint.2016.03.069>
49. Park YH, Park SY, In I (2015) Direct noncovalent conjugation of folic acid on reduced graphene oxide as anticancer drug carrier. *J Ind Eng Chem* 30:190–196. <https://doi.org/10.1016/j.jiec.2015.05.021>
50. Yun H, Ahmed MS, Lee K, Jeon S, Lee CW (2016) Potential enhancement of antibacterial activity of grapheneoxide-silver nanocomposite by introducing C2carbon chain linkage. *Appl Surf Sci* 360:915–920. <https://doi.org/10.1016/j.apsusc.2015.11.084>
51. Krishnamoorthy K, Veerapandian M, Yun K, Kim SJ (2013) The chemical and structural analysis of graphene oxide with different degrees of oxidation. *Carbon* 53:38–49. <https://doi.org/10.1016/j.carbon.2012.10.013>
52. Li J, Wang G, Zhu H, Zhang M, Zheng X, Di Z, Liu X, Wang X (2014) Antibacterial activity of large-area monolayer graphene film manipulated by charge transfer. *Sci Rep* 4:4359. <https://doi.org/10.1038/srep04359>
53. Cui J, Yang Y, Hu Y, Li F (2015) Rice husk based porous carbon loaded with silver nanoparticles by a simple and cost-effective approach and their antibacterial activity. *J Colloid Interface Sci* 455:117–124. <https://doi.org/10.1016/j.jcis.2015.05.049>
54. Chang YN, Gong JL, Zeng GM, Ou XM, Song B, Guo M, Zhang J, Liu HY (2016) Antimicrobial behavior comparison and antimicrobial mechanism of silver coated carbon nanocomposites. *Process Saf Environ Prot* 102:596–605. <https://doi.org/10.1016/j.psep.2016.05.023>
55. Lan NT, Chi DT, Dinh NX, Hung ND, Lan H, Tuan PA, Thang LH, Trung NN, Hoa NQ, Huy TQ, Quy NV, Duong TT, Phan VN, Le AT (2014) Photochemical decoration of silver nanoparticles on graphene oxide nanosheets and their optical characterization. *J Alloys Compd* 615:843–848. <https://doi.org/10.1016/j.jallcom.2014.07.042>
56. Pant B, Pokharel P, Tiwari AP, Saud PS, Park M, Ghouri ZK, Choi S, Park SJ, Kim HY (2015) Characterization and antibacterial properties of aminophenol grafted and Ag NPs decorated graphene nanocomposites. *Ceram Int* 41:5656–5662. <https://doi.org/10.1016/j.ceramint.2014.12.150>
57. Joshi PN, Agawane S, Athalye MC, Jadhav V, Sarkar D, Prakash R (2017) Multifunctional inulin tethered silver-graphene quantum dots nanotheranostic module for pancreatic cancer therapy. *Mater Sci Eng, C* 78:1203–1211. <https://doi.org/10.1016/j.msec.2017.03.176>
58. Byeon HJ, le Thao Q, Lee S, Min SY, Lee ES, Shin BS, Choi HG, Youn YS (2016) Doxorubicin-loaded nanoparticles consisted of cationic- and mannose-modified-albumins for dual-targeting in brain tumors. *J Control Release* 225:301–313. <https://doi.org/10.1016/j.jconrel.2016.01.046>
59. Gessner A, Waicz R, Lieske A, Paulke BR, Mäder K, Müller R (2000) Nanoparticles with decreasing surface hydrophobicities: influence on plasmaprotein adsorption. *Int J Pharm* 196:245–249. [https://doi.org/10.1016/S0378-5173\(99\)00432-9](https://doi.org/10.1016/S0378-5173(99)00432-9)
60. Sarika PR, James NR (2016) Polyelectrolyte complex nanoparticles from cationised gelatin and sodium alginate for curcumin delivery. *Carbohydr Polym* 148:354–361. <https://doi.org/10.1016/j.carbpol.2016.04.073>
61. Lv Y, Tao L, Bligh SWA, Yang H, Pan Q, Zhu L (2016) Targeted delivery and controlled release of doxorubicin into cancer cells using

- a multifunctional graphene oxide. *Mater Sci Eng, C* 59:652–660. <https://doi.org/10.1016/j.msec.2015.10.065>
62. Elvira C, Gallardo A, Roman JS, Cifuentes A (2005) Covalent polymer-drug conjugates. *Molecules* 10:114–125. <https://doi.org/10.3390/10010114>
63. Wang X, Li C, Fan N, Li J, He Z, Sun J (2017) Multimodal nanoporous silica nanoparticles functionalized with aminopropyl groups for improving loading and controlled release of doxorubicin hydrochloride. *Mater Sci Eng, C* 78:370–375. <https://doi.org/10.1016/j.msec.2017.04.060>
64. Yang X, Zhang X, Liu Z, Ma Y, Huang Y, Chen Y (2008) High-efficiency loading and controlled release of doxorubicin hydrochloride on graphene oxide. *J Phys Chem C* 112:17554–17558. <https://doi.org/10.1021/jp806751k>
65. Lee YK, Choi J, Wang W, Lee S, Nam TH, Choi WS et al (2013) Nullifying tumor efflux by prolonged endolysosome vesicles: development of low dose anticancer carbon nanotube drug. *ACS Nano* 7:8484–8497. <https://doi.org/10.1021/nn4041206>
66. Li R, Wu R, Zhao L, Hu Z, Guo S, Pan X, Zou H (2011) Folate and difunctionalized multiwall carbon nanotubes as dual-targeted drug nanocarrier to cancer cells. *Carbon* 49:1797–1805. <https://doi.org/10.1016/j.carbon.2011.01.003>
67. Bayda S, Hadla M, Palazzolo S, Kumar V, Caligiuri I, Ambrosi E et al (2017) Bottom-up synthesis of carbon nanoparticles with higher doxorubicin efficacy. *J Control Release* 248:144–152. <https://doi.org/10.1016/j.jconrel.2017.01.022>
68. Zhang X, Meng L, Lu Q, Fei Z, Dyson PJ (2009) Targeted delivery and controlled release of doxorubicin to cancer cells using modified single wall carbon nanotubes. *Biomaterials* 30:6041–6047. <https://doi.org/10.1016/j.biomaterials.2009.07.025>
69. Fu Y, Kao WJ (2010) Drug release kinetics and transport mechanisms of nondegradable and degradable polymeric delivery systems. *Expert Opin Drug Deliv* 7:429–444. <https://doi.org/10.1517/17425241003602259>
70. Sun X, Liu Z, Welsher K, Robinson JT, Goodwin A, Zaric S, Dai H (2008) Nano-graphene oxide for cellular imaging and drug delivery. *Nano Res* 1:203–212. <https://doi.org/10.1007/s12274-008-8021-8>
71. Yang K, Wan J, Zhang S, Zhang Y, Lee ST, Liu Z (2011) *In vivo* pharmacokinetics, long-term biodistribution, and toxicology of PEGylated graphene in mice. *ACS Nano* 5:516–522. <https://doi.org/10.1021/nn1024303>
72. Chen J, Liu H, Zhao C, Qin G, Xi G, Li T, Wang X, Chen T (2014) One-step reduction and PEGylation of graphene oxide for photothermally controlled drug delivery. *Biomaterials* 35:4986–4995. <https://doi.org/10.1016/j.biomaterials.2014.02.032>
73. Justin R, Tao K, Román S, Chen D, Xu Y, Geng X et al (2016) Photoluminescent and superparamagnetic reduced graphene oxide–iron oxide quantum dots for dual-modality imaging, drug delivery and photothermal therapy. *Carbon* 97:54–70. <https://doi.org/10.1016/j.carbon.2015.06.070>
74. Horcajada P, Chalati T, Serre C, Gillet B, Sebrie C, Baati T et al (2010) Porous metalorganic-framework nanoscale carriers as a potential platform for drug delivery and imaging. *Nat Mater* 9:172–178. <https://doi.org/10.1038/nmat2608>

Publisher's Note Springer Nature remains neutral with regard to jurisdictional claims in published maps and institutional affiliations.